Romanian Reports in Physics **71**, 714 (2019)

CORRELATIONS BETWEEN GEOMAGNETIC ANOMALIES RECORDED AT MUNTELE ROSU SEISMIC OBSERVATORY (ROMANIA) AND SEISMICITY OF VRANCEA ZONE

A. MIHAI[1,2], I.A. MOLDOVAN[1], V.E. TOADER[1], M. RADULIAN[1], A.O. PLACINTA[1]

[1] National Institute for Earth Physics, RO-077825, Calugareni st, no 12, Magurele, Ilfov, Romania
[2] Faculty of Physics, University of Bucharest, Atomistilor 405, POB MG-11, RO-077125, Bucharest-Magurele, Romania
E-mail: *mihai.a.andrei@gmail.com*

Received October 4, 2018

Abstract. In the present paper, a relationship between geomagnetic anomalies recorded at one magnetometer located inside Vrancea seismogenic zone and the occurrence of intermediate earthquakes is examined. To better distinguish the regional anomalies from global geomagnetic storms, the datasets were correlated with the geomagnetic indices taken from NOAA/Space Weather Prediction Center. During five years of investigations (2013–2018), three intermediate depth earthquakes with a moment magnitude M_w larger than 5.0 occurred in the Vrancea zone and were accompanied by significant anomalies on the E-W component of the local geomagnetic field (B_y) measured at Muntele Rosu (MLR) Observatory. The anomalies recorded at MLR were also analyzed along with the seismic energy distribution, providing good opportunity to distinguish the anomaly morphology, and were correlated with the radon emissions and temperature variations, during the detector operating time, in 2016.

Key words: geomagnetic anomalies, intermediate earthquakes, Vrancea zone.

1. INTRODUCTION

The Vrancea region is one of the most active seismic zones in Europe and it is known for its strong intermediate-depth earthquakes. This area is a complex seismic region situated at the convergence of three major tectonic units: (i) East European Craton to the Northeast, (ii) Moesian plate to the South and (iii) the younger Intra-Alpine plates (Tisza-Dacia blocks) to the West.

The Vrancea seismogenic zone is characterized by both crustal and intermediate earthquakes. Crustal activity (0–40 km) in Vrancea zone is weak, with an activity rate of 0.514, for the earthquake with $M_w > 3$ [1], while the intermediate activity is high, with an activity rate of 100.1 events per year for earthquakes with $M_w > 3$.

The present paper comes to complete the study of [2] with the radon emissions data and in correlation with intermediate depth Vrancea seismicity (Table 1) and the geomagnetic anomalies recorded on MLR observatory, during a five years period 1.01.2013–1.01.2018. More than that, the released seismic energy was computed during the geomagnetic anomalies in order to see if there exists a quantitative link between anomaly drop and seismic activity. If in the previous study were used the geomagnetic data sets to demonstrate a relation between the drop of E-W horizontal magnetic (B_y) component and the seismic activity, now will be used extra-data and to obtain a more reliable earthquake forecasting.

Table 1

M_w > 5.0 subcrustal earthquakes occurred in Vrancea during 2013–2018

No	Data/hour	Lat (N)	Long (E)	*H* (km)	M_w	D_{MLR} (km)
Eq. 1	06.10.2013/01:37	45.67	26.58	135.1	5.2	50
Eq. 2	23.09.2016/23:11	45.71	26.61	92	5.5	56
Eq. 3	27.12.2016/23:20	45.71	26.60	96.9	5.6	55

Anomalous geomagnetic anomalies were observed prior to earthquakes occurrences [3, 4, 5, 6, 7]. A pair of magnetometers station located in Peru recorded some unipolar pulses prior to earthquakes [8], but these unipolar pulses looks similar to pulses created by lightning phenomena. One proposed source for these pulses is the break-up of peroxy defects as result of an increase of tectonic stress. Silicate minerals can form peroxy defects that are typically introduced through the incorporation of H_2O into anhydrous minerals, and these peroxy defects act like a source of electron and positive holes, generates currents that can disturb the local magnetic field. Piezomagnetic phenomena could also create anomalous signals as a response of crustal deformation applied to ferromagnetic minerals [9]. A long-term anomaly variation was detected before and during the Molise Earthquakes at L'Aquila station situated 140 km away from epicenter [5]. This anomaly shows a decrease of ~ 40 nT only on *H* component (North-South component) and looks very similar to the anomalies recorded in Vrancea [2, 10]. There are two similarities and two differences regarding these two types of anomalies, both of them present a drop of one magnetic horizontal component and also the morphology of anomalies looks similar. The main difference between two cases is represented by the depth of earthquakes that accompanied the anomalies. The L'Aquila anomaly occurs prior to crustal events and for Vrancea zone, only the intermediate earthquakes are accompanied by anomalies [2]. The last difference is represented by the distance between magnetic observatories and seismic zones, which is significantly smaller for Vrancea case.

Other papers [11] demonstrated that rocks with significant amounts of mafic/ ultramafic composition may account for some magnetic anomalies. To see the magnetic susceptibility variance with temperature the unweathered samples were heated and then cooled in a normal atmosphere (oxygenated atmosphere) but also in an argon atmosphere to simulate the deep earth conditions. It was noticed that susceptibility decrease drastically when the Currie temperature was reached. During the cooling process, the samples take back their magnetic properties but not at the same values.

Most rocks contain a small concentration of radon, and there are reports of spikes in radon concentrations prior to major earthquakes due to pre-seismic stress and rocks fracturing which releases it. Radon concentration was monitored by [12] in five stations and noticed some variations in radon concentration before three moderate earthquakes, but the cause of this variations may be related to weather changes: rainfall, atmospheric pressure, temperature, humidity, wind, groundwater.

2. DATA AND EQUIPMENT

Starting with 1996, the Romanian Seismic Network was improved and extended with a Multidisciplinary Network designed for geophysical/geochemical and atmospheric field parameter monitoring and event detection, network that includes recordings of magneto-telluric and electric-electrostatic field, ULF waves, air ionization, radon and CO, infrasound, etc. [6, 7].

The Muntele Rosu (MLR) observatory location, near to Western wedge of Vrancea seismogenic zone provides a good opportunity to study the local geomagnetic anomalies for the 2013–2018 period. All five years of data were taken from Muntele Rosu (MLR) observatory and compared with geomagnetic data from Surlari (SUA) to distinguish the local geomagnetic data. The magnetometer from MLR was installed inside a tunnel to avoid the temperature variations of the instruments. The location also provides a good sealing properties for others anthropic effects like railways, roads, buildings etc. Throughout 2016 year, a radon detector was installed in the tunnel and gives us the opportunity to compare the radon readings with geomagnetic anomalies associated to two of the largest earthquakes occurred during the study period (Eq. 2 and Eq. 3 from Table 1).

In this study were used the following data:

(*i*) The geomagnetic data from 2013–2018 were taken from Surlari (SUA) part of international network INTERMAGNET, and from Muntele Rosu (MLR) part of National Institute for Earth Physics;

(*ii*) The seismic bulletins used in this study were taken from "Romplus" seismic catalog developed by National Institute for Earth Physics;

(*iii*) The planetary K-index used to characterize the magnitude of geomagnetic storms were taken from the National Oceanic and Atmospheric Administration (NOAA)/ Space Weather Prediction Center;

(*iv*) Temperature and radon measurements used in this study cover a year period length and provide to the present paper only one anomaly associated with the largest earthquakes (Eq. 2 and Eq. 3 from Table 1) recorded during 2016.

The MLR magnetometer is a three-axis fluxgate type developed by Bartington Instruments with a measuring range of +/– 70μT. The magnetic field sensor is sensitivity to small variations with a band larger than 2 kHz but up to 3 kHz and 15 pT rms/(Hz$^{1/2}$) noise. Same company designed the data-logger acquisition which have six channels and a resolution of 24-bits. The sampling of Data-logger acquisition is controlled by a software program and displays the average of 12 samples recorded in one minute. For radon measurements were used Radon Scout produced by Sarad company, with a measurements range 0–10 Mbq/m^3 and a sensitivity of 5.52 cph/(kB/m^3). The instrument uses the X-ray spectroscopy with PIN diodes and has an integration interval of 1 hour or to 3 hours.

Seismic energy calculation was made by using a software tool called “Report energy” [13] (LabVIEW program) which calculate the cumulative energy (Fig. 1) using the bulletins generated by Antelope software (http://ds.iris.edu/ds/nodes/dmc/software/downloads/Antelope/) as input parameters.

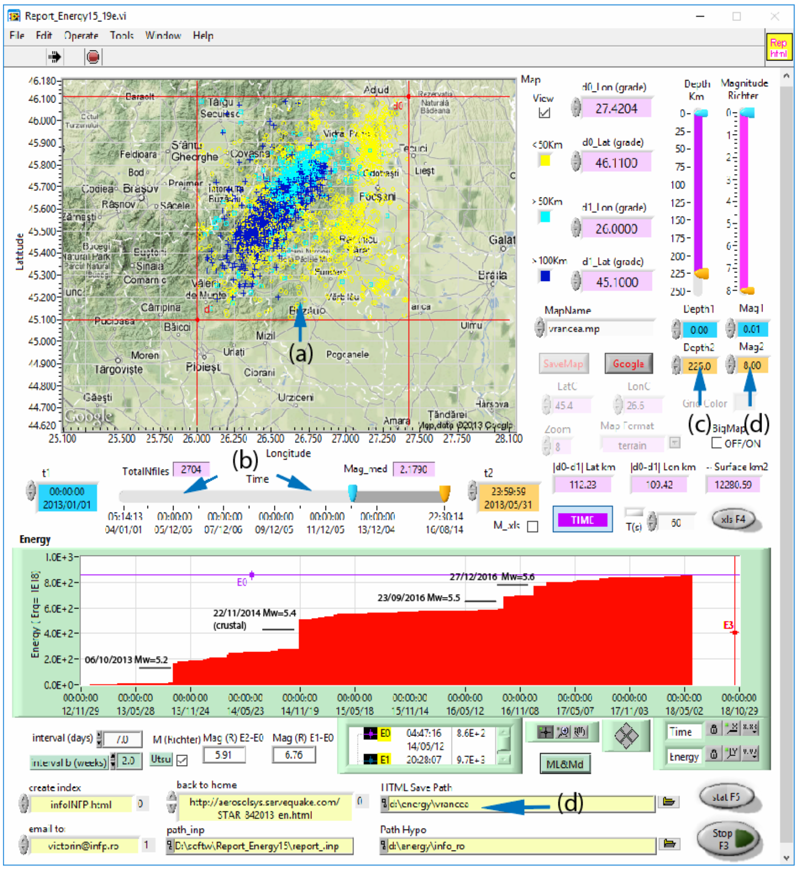

Fig. 1 – Cumulative seismic energy evolution for Vrancea zone from 29.11.2012 to 02.05.2018.

Firstly, it is necessary to set parameters like: (a) seismic area, (b) time interval, (c) depth interval, (d) magnitude interval and (e) the location path of seismic bulletins. Each earthquake located inside the seismic area is converted in energy using Equation (1) and cumulated with the seismic energy of all previous days from the time interval. Equation (2) is necessary to obtain M_s (Surface magnitude) using the M_l (Local magnitude) magnitudes generated by Antelope program. This program was previously used by [13] to separate the regional/local seismic areas and the precursor situations using the earthquake energy. The cumulative energy graphs are used to compare the geomagnetic anomalies decrease with the earthquake energy release. Thus, alongside cumulative seismic energy we also plot the graphs with daily energy release using the Eq. (3)

$$\lg (E) = 11.8 + 1.5 \cdot M_s \tag{1}$$

$$M_l = -2.14 + 1.43 \cdot M_l - 0.018 \cdot M_l^2 \tag{2}$$

$$\lg (E) = 11.8 + 1.5 \cdot M_l \tag{3}$$

The global magnetic variations represent the main phenomena that disturb the magnetic measurements on sites. These variations are represented by the solar storms which creates an increase in amplitude and frequency of geomagnetic representation. To avoid the false identification of these solar storms as seismo-magnetic anomalies, the representation of geomagnetic field was represented alongside the daily sum of K_p indices. For graphical reasons, the K_p indices measured at every 3 hours were represented as daily sum, so the solar storms were well defined when the sum of K_p indices exceed the value 20. The quantity of solar radiation increases during summer time and decrease during winter, these phenomena make the diurnal variation uneven. Creating a lunar representation of geomagnetic field on MLR observatory was helpful to note that big diurnal variation can influence the detection of small anomalies.

The missing data sets recorded at MLR observatory were corrected automatically using a LabVIEW program which replaces the missing data with the last good value. Missing data sets recorded at SUA (INTERMAGNET Observatory) were replaced with the number “99999” to highlight the malfunction time of instruments. For graphical reasons, this value was also replaced with the last good recorded value.

Personnel visits or maintenance operations at the location could also to generate false variations in geomagnetic filed. This kind of anomalies lasts only a short time and are visible on all magnetic components and bring with them a significant increase of magnetic field. These anthropic anomalies were removed using a LabVIEW program.

3. RESULTS AND DISCUSSION

To highlight the local geomagnetic anomalies recorded at MLR observatory, the data from Surlari Observatory (SUA) were also plotted, as reference data. During the studied 5 years period, [2] has centralized 8 anomalies in Table 2, together with seismic sequences that accompanied these anomalies, seismological parameters, K_p indices, magnetic component affected, shape and B_y component drop evolution. The daily sum of K_p indices was plotted alongside geomagnetic data, to avoid the false identification of solar storms as seismo-magnetic anomalies. As shown in Fig. 2, the presence of solar storms is pointed when the sum of K_p indices reach the redline. On geomagnetic representations, the solar storms are accompanied by an increase in frequency and amplitude.

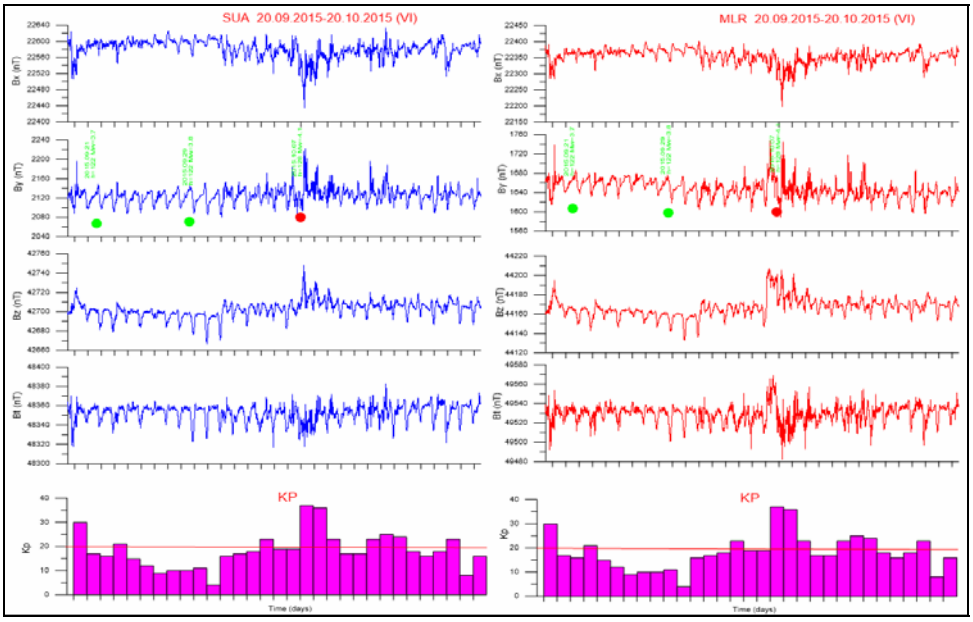

Fig. 2 – (Color online). Anomaly number VI (Table 2) on MLR B_y component and the earthquakes that occurred during this anomaly and the daily representation of K_p indices.

Figure 2 presents the shortest anomaly (VI from Table 2), where the magnetic field on horizontal component B_x and on the vertical component B_z, looks similar for both observatories MLR and SUA. The only one notable variation is on horizontal component, B_y. Associated with geomagnetic anomalies number I, II, III, VI and VII from Table 2, in Figs. 2, 3 and 4 it is also illustrated the seismicity, represented by colored bullets, with the same color as in Table 2. With green bullets are represented the earthquakes that occurred on the fall of the B_y magnetic component and are called generic “head-earthquakes”. After the B_y component drop, inside geomagnetic morphology, it could be recognized a period of stagnation of B_y component. This period could also be accompanied by earthquakes, named “middle-earthquakes (red bullets). The “tail-earthquakes” are the last earthquakes and are associated with a return of B_y magnetic field component. As can be seen in Table 2, the anomalies could be short period (I, III, IV, V, VI anomalies) and long period (II, VII anomalies).

Table 2

The seismic sequences (I–VII) with seismological parameters and K_p indices of all Vrancea earthquakes of magnitude $M_w > 3$ that occurred alongside the geomagnetic anomalies [2]

DATE	TIME	LATITUDE	LONGITUDE	DEPTH	ΣKp	Mw	Magnetic component affected	Types of earthquakes	Shape of anomaly
I									
18/09/2013	0:27:28	45.67	26.57	149.9	14	3.6	By	head earthquake	Short time anomaly with a decrease of ~40nT
06/10/2013	1:37:21	45.67	26.58	135.1	7	5.2	By	middle earthquake	
15/10/2013	19:33:12	45.62	26.55	141.5	31	4.4	By	tail earthquake	
22/10/2013	7:16:50	45.75	26.69	132	8	3.6	By	tailearthquake	
II									
14/11/2013	21:44:32	45.5	26.26	124.2	4	3.6	By	head earthquake	Long anomaly with a decrease of ~40nT. The earthquakes are present along the decreasing trend (head earthquakes), when the trend is steady (middle earthquakes) and when the magnetic anomaly trend increase (tail earthquakes). This anomaly decrease in steps having two series of head earthquakes.
21/11/2013	6:38:53	45.76	26.71	89	2	4.3	By	head earthquake	
28/11/2013	04:21.6	45.56	26.4	126.7	2	3.7	By	head earthquake	
05/12/2013	1:24:52	45.65	26.47	120.3	9	3.4	By	head earthquake	
05/12/2013	3:48:24	45.51	26.38	118.9	9	3.2	By	head earthquake	
09/12/2013	17:55:45	45.69	26.48	94.2	6	3.4	By	head earthquake	
27/12/2013	7:58:32	45.74	26.65	93	6	3.5	By	middle earthquake	
29/12/2013	19:22:12	45.65	26.44	151.7	9	3.8	By	middle earthquake	
12/01/2014	18:26:02	45.5129	26.4293	137.2	13	4.1	By	head earthquake`	
23/01/2014	6:15:05	45.4877	26.2537	132.3	12	4.4	By	head earthquake`	
24/01/2014	13:11:40	45.5867	26.5601	87.6	7	3.5	By	head earthquake`	
03/02/2014	0:26:31	45.6657	26.5202	139.2	12	4	By	middle earthquake	
24/02/2014	22:54.2	45.7414	26.6735	104	12	4.1	By	tail earthquake	
26/03/2014	19:46:29	45.6578	26.5406	133.3	14	4.2	By	tailearthquake	
29/03/2014	1:55:17	45.3462	26.2306	144.1	17	4	By	tailearthquake	
29/03/2014	19:18:05	45.6094	26.4709	134.4	17	4.6	By	tailearthquake	
31/03/2014	15:48:47	45.5751	26.4742	139.7	14	3.5	By	tailearthquake	
03/04/2014	12:38:57	45.4924	26.4003	127.9	13	4.3	By	tailearthquake	
07/04/2014	12:59:53	45.486	26.2667	112.3	17	3.8	By	tailearthquake	
11/04/2014	20:33:55	45.6311	26.4518	149.9	15	3.6	By	tailearthquake	
III									
22/12/2014	0.6858155	45.5457	26.4405	141.3	20	3.7	By	head earthquake	Short time anomaly with a decrease of ~20nT
24/12/2014	0.2629846	45.6853	26.6021	136.1	21	3.7	By	head earthquake	
03/01/2015	3:39:35	45.7782	26.6848	78.7	21	3.8	By	middle earthquake	
03/01/2015	10:08:45	45.4843	26.3674	138.4	21	3.7	By	middle earthquake	
04/01/2015	40:38.6	45.532	26.3744	120.2	20	4.1	By	middle earthquake	
14/01/2015	3:10:54	45.5501	26.3503	145.9	12	3.9	By	tailearthquake	
24/01/2015	7:55:47	45.7123	26.5712	88.4	11	4.3	By	tailearthquake	
28/01/2015	22:52:00	45.6405	26.494	128.7	11	3.8	By	tailearthquake	
IV									
28/01/2015	22:52:00	45.6405	26.494	128.7	11	3.8	By	head earthquake	Short time anomalie with a decrease of ~10nT
31/01/2015	22:47:35	45.6615	26.5441	148.5	13	3.1	By	head earthquake	
16/02/2015	19:34:12	45.634	26.5805	161.2	9	3.5	By	middle earthquake	
21/02/2015	19:10:13	45.6883	26.5791	141.3	16	3.8	By	middle earthquake	
27/02/2015	11:40.1	45.725	26.6709	129.6	5	3.9	By	tailearthquake	
V									
13/03/2015	22:31:19	45.5769	26.5355	118	10	3.7	By	middle earthquake	Short time anomalie with a decrease of ~10nT
15/03/2015	16:54:17	45.8038	26.9305	74.3	15	3.6	By	middle earthquake	
16/03/2015	15:49:49	45.5991	26.4484	118.2	18	4.3	By	tailearthquake	
27/03/2015	21:48:34	45.7861	26.6929	115.2	15	3.5	By	tailearthquake	
29/03/2015	0:44:58	45.6193	26.478	145.4	19	4.3	By	tailearthquake	
VI									
29/09/2015	53:49.1	45.7189	26.719	121.6	11	3.8	By	head earthquake	Short time anomalie with a decrease of ~10nT
07/10/2015	25:02.4	45.6621	26.8539	128.5	37	4.1	By	middle earthquake	
VII									
16/09/2016	9:10:57	45.6458	26.5912	140.8	16	3.5	By	head earthquake	Long anomaly with a decrease of ~100nT. The earthquakes are present along the decreasing trend (head earthquakes), when the trend is steady (middle earthquakes) and when the magnetic anomaly trend increase (tail earthquakes). This anomaly decrease in steps having two series of head earthquakes.
22/09/2016	7:18:45	45.658	26.5249	132.4	10	3.5	By	head earthquake	
23/09/2016	23:11:20	45.7148	26.6181	92	7	5.5	By	head earthquake	
16/10/2016	56:26.7	45.4762	26.3303	126	21	3.5	By	middle earthquake	
23/10/2016	3:10:34	45.631	26.4711	144.5	0	3.5	By	middle earthquake	
31/10/2016	11:59:50	45.8425	26.776	90.8	16	4	By	middle earthquake	
19/11/2016	11:30:39	45.6411	26.5083	140.8	6	4.1	By	middle earthquake	
30/11/2016	13:34:38	45.6814	26.5821	137	5	3.6	By	middle earthquake	
01/12/2016	9:01:20	45.832	26.8612	97.5	7	3.5	By	middle earthquake	
10/12/2016	7:31:31	45.5634	26.5405	128.5	19	3.5	By	head earthquake`	
17/12/2016	4:49:04	45.4986	26.096	70.7	8	3.5	By	head earthquake`	
17/12/2016	11:16:06	45.4924	26.3877	120.2	8	3.7	By	head earthquake`	
27/12/2016	23:20:56	45.7139	26.5987	96.9	16	5.6	By	head earthquake`	
05/01/2017	23:55.7	45.66	26.5317	141.6	23	3.7	By	head earthquake`	
05/01/2017	13:16:10	45.6339	26.5096	140.7	23	3.6	By	head earthquake`	
05/01/2017	14:47:44	45.7596	26.7259	114.4	23	3.7	By	head earthquake`	
06/01/2017	14:01:11	45.7001	26.6539	138.2	22	3.5	By	head earthquake`	
08/02/2017	9:52:06	45.6955	26.6727	129.9	8	4.1	By	tailearthquake	
08/02/2017	15:08:21	45.4874	26.2849	123.2	8	4.8	By	tailearthquake	
22/02/2017	9:29:45	45.6576	26.7623	139.3	15	3.5	By	tailearthquake	

During the five years of observation, four earthquakes with M_w larger than 5 occurred in Vrancea zone. Three of them were intermediate earthquakes (Eq. 1–Eq. 3, in Table 1) and were accompanied by B_y component drop. The crustal earthquake with $M_w = 5.4$ occurred on November 22, 2014, was not accompanied by a geomagnetic anomaly. So, the anomalies related to MLR, B_y horizontal component are related to deep processes that occurred at high depths [2]. The cumulative energy represented in Fig. 1 shows an increase in steps when a major earthquake occurs. Four major jumps are visible from 2013 till the 2018 year. The main reason for these jumps are the occurrence of earthquakes with $M_w > 5$, and the jumps are missing for the 2015 and 2017 years, years with a low seismic activity.

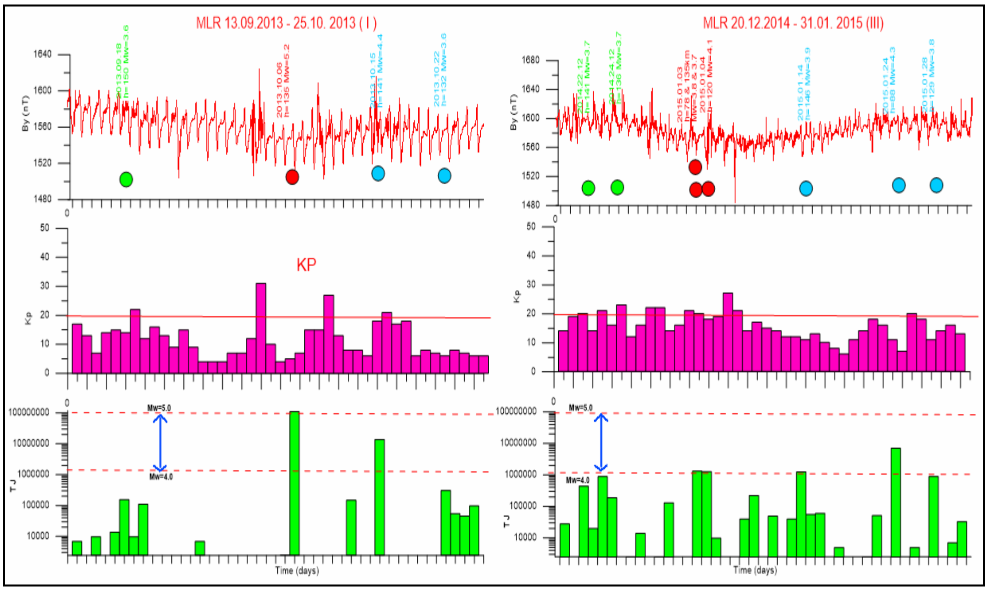

Fig. 3 – (Color online). Representation of two short-period geomagnetic anomalies (anomaly number I and III) recorded on B_y component alongside the daily seismic energy (green histograms), and K_p indices (pink histograms).

Figure 3 illustrates the seismicity (colored dots), the daily sum of K_p indices and daily energy release for 2 short period anomalies taken from Table 2. Anomalies I and III show the same decrease on B_y component at around 40 nT, but the seismic activity highlighted by daily energy representation look different. In anomaly number I, the energy was released mostly through a single larger earthquake (Eq. 1, $M_w = 5.2$), surrounded by gaps in seismicity. Instead, the anomaly number III shows a more homogeneous seismicity, with no significant gaps and a large number of smaller earthquakes.

The same situation is also noticeable for long-term anomalies (Fig. 4). Anomaly number II shows a decrease of ~40 Nt recorded on B_y component and the anomaly number VII shows a greater drop of B_y component (90 nT). Also, the seismicity and the energy release during these anomalies look different, with greater seismic activity for the anomaly number 7. Studying the seismic energy, the drop on B_y component is proportional with the seismic activity. Using the daily seismic energy and the cumulative seismic energy alongside geomagnetic data during anomalies presence could help to make an approximative idea about how earthquakes grow.

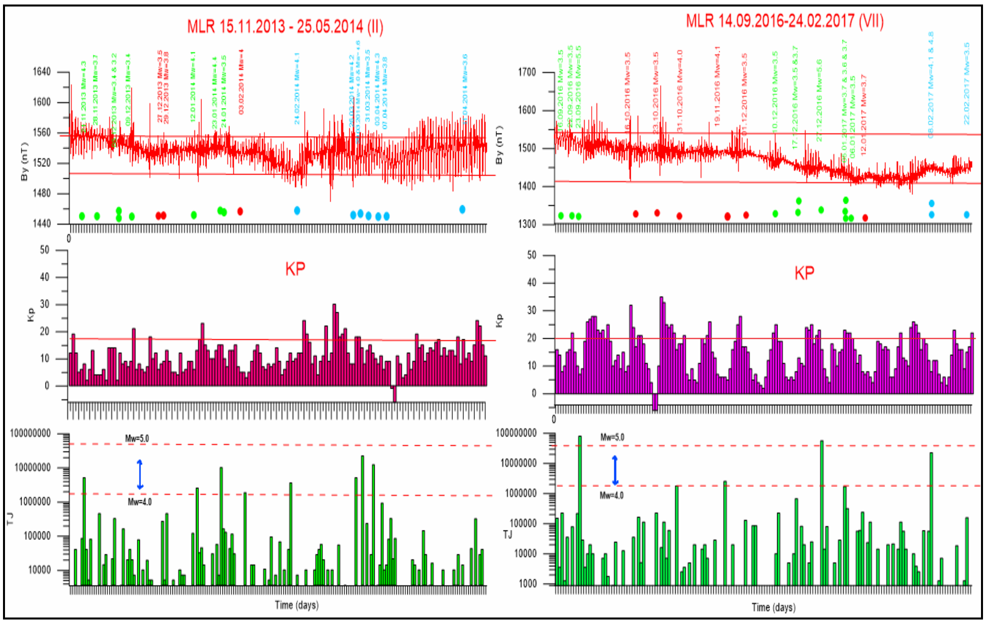

Fig. 4 – Representation of two long-period geomagnetic anomalies (anomaly number II and VII) recorded on B_y component alongside with the K_p indices (pink histograms) and the daily seismic energy (green histograms).

Radon emissions recorded at MLR observatory show no clear relation with medium size (M_w < 6.0) earthquake occurrence (Fig. 5). Radon emissions look to be related more to other factors like humidity, raining periods and groundwater circulation through the tunnel. It is known that radon ascends to the surface mainly through cracks and faults, on short distances by diffusion and long distances by advection (dissolved in water or carrier gases) [14]. The main uncertainty for Vrancea zone, remains the migration time and the migration paths from the earthquake focus to the surface. The anomalies presence only on B_y component can be explained due to instrument setup, which gives low readings on B_y component (1600 nT) and makes the anomaly visible. For example, an anomaly with 40 nT drop on B_y gives on the total horizontal field a comparative anomaly of 2–3 nT, which make impossible to see a variance on total horizontal field. The anomalies recorded on MLR observatory could be explained probably by a magnetic signature of serpentinization reactions or partial melts of rocks bodies from deep depth (intermediate depth) [2].

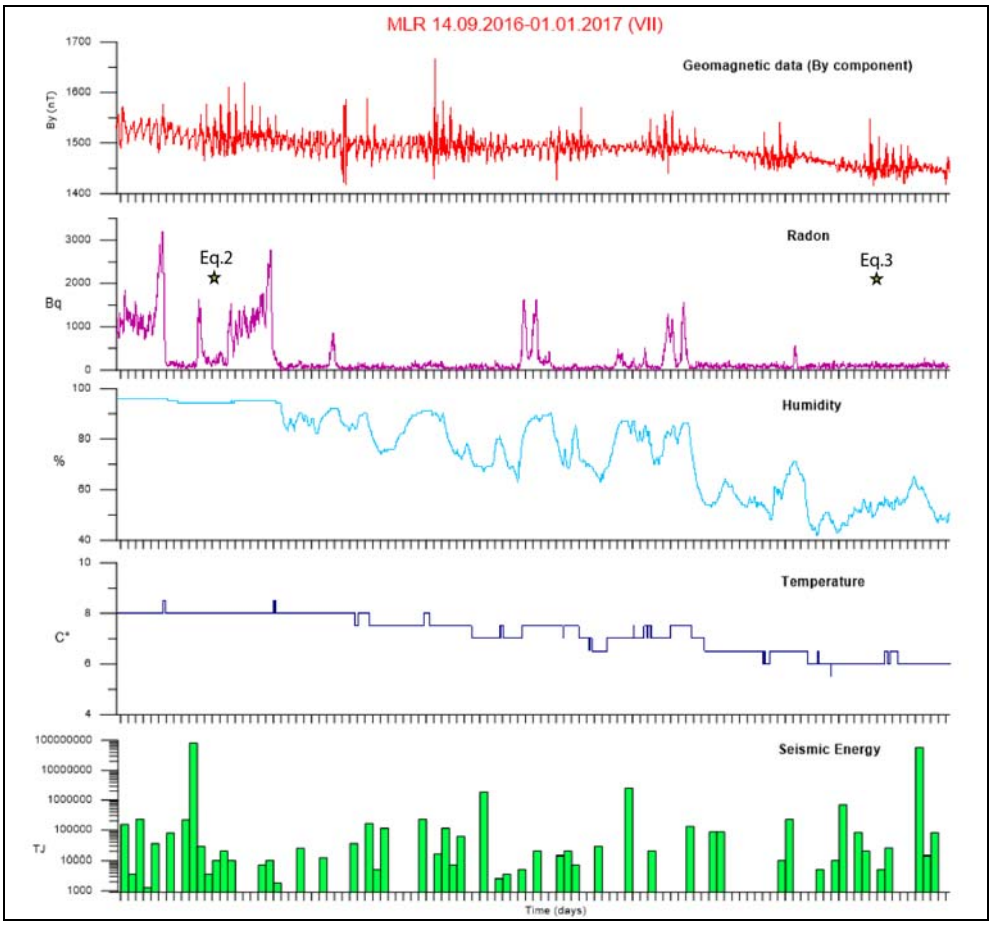

Fig. 5 – Correlation between seismic energy, temperature, humidity and radon readings recorded at MLR observatory during anomaly number VII.

4. CONCLUSION

The main propose of this study was to correlate the geomagnetic anomalies recorded at MLR observatory in the last 5 years with seismicity, seismic energy, and radon readings. The three major intermediate earthquakes occurred in this interval provided a good opportunity to investigate the link between seismicity in Vrancea zone and the presence of anomalies recorded at MLR observatory, the seismic energy distribution, and radon emissions.

The radon emissions couldn't be related to the seismic activity, the main peaks in radon measurements were probably triggered by weather phenomena which change the humidity and groundwater circulation. The degree of B_y component drop is directly proportional with the released seismic energy. Big drops on B_y components can be followed by big earthquakes but also small and short anomalies can be followed by a significant event/s. For a better forecasting, the futures earthquakes that will be accompanied an anomaly needs the study of seismic energy. The results of this paper could be used as a benchmark for the future anomalies, and the future anomalies will reshape these results. The crustal earthquakes that occur on November 22, 2014, was not accompanied by a geomagnetic anomaly, placing the disruptive processes at high depth. Intermediate earthquakes occurrences seem to be related to partial melts of rocks at the contact with Vrancea slab which create a magnetic signature readable on B_y horizontal component.

Acknowledgments. This paper was supported from Nucleu Program PN 19 080102/2019. The results presented in this paper rely on the data collected at *Surlari (SUA)*. We thank *Geological Institute of Romania*, for supporting its operation and INTERMAGNET for promoting high standards of magnetic observatory practice.

REFERENCES

1. I.A. Moldovan, E. Popescu and A. Constantin, *Probabilistic seismic hazard assessment in Romania: application for crustal seismic active zones,* Rom. Journ. Phys. **53**, 575–591 (2008).
2. A. Mihai, I.A. Moldovan, V. Toader, L. Petrescu, R. Partheniu, *Geomagnetic field behaviour at Muntele Rosu (Romania) and anomaly interpretation*, IOP Conf. Ser.: Earth Environ. Sci. **221**, 012055 (2019).
3. I.A. Moldovan, A.S. Moldovan, C.G. Panaiotu, A.O. Placinta, and Gh. Marmureanu, *The geomagnetic method on precursory phenomena associated with 2004 significant intermediate Vrancea seismic activity*. Rom. Journ. Phys. **54**, 249–261 (2009).
4. K. Yumoto, S. Ikemoto, M.G. Cardinal, M. Hayakawa, K. Hattori, J.Y. Liu, S. Saroso, M. Ruhimat, M. Husni, D. Widarto, and E.A. Ramos, *A new ULF wave analysis for Seismo-Electromagnetics using CPMN/MAGDAS data,* Phys. Chem. Earth **34**, 360–6 (2009).
5. E.M. Takla, K. Yumoto, P.R. Sutcliffe, V. Nikiforov, and R. Marshall, *Possible association between anomalous geomagnetic variations and the Molise Earthquakes at Central Italy during 2002,* Phys. Earth Planet. Int. **185**, 29–35 (2011).
6. V.E. Toader, I.A. Moldovan, A. Marmureanu, and C. Ionescu. *Detection of events in a multidisciplinary network monitoring Vrancea area*, Rom. Journ. Phys. **61**, 1437–1449 (2016).
7. V.E. Toader, I.A. Moldovan, and C. Ionescu. *Complex monitoring and alert system for seismotectonic phenomena,* Rom. Journ. Phys. **60**, 1225–1233 (2015).
8. J. Scoville, J. Heraud, and F. Freund, *Pre-earthquake magnetic pulses,* Nat. Hazards Earth Syst. Sci. **15**, 1873–1880 (2015).
9. K.I. Yamazaki, *Calculation of the piezomagnetic field arising from uniform regional stress in inhomogeneously magnetized crust,* Earth Planets Space **61**, 1163–8 (2009).
10. I.A. Moldovan, A.O. Placinta, A.P. Constantin, A.S. Moldovan, and C. Ionescu, *Correlation of geomagnetic anomalies recorded at Muntele Rosu Seismic Observatory (Romania) with earthquake occurrence and solar magnetic storms,* Ann. Geophys. **55**, 125–137 (2012).

11. E. Strada, F.M. Talarico, and F. Florindo, *Magnetic petrology of variably retrogressed eclogites and amphibolites: A case study from the Hercynian basement of northern Sardinia (Italy),* J. Geophys. Res. Solid Earth **111,** B12 (2006).
12. V.E. Toader, I.A. Moldovan, A. Marmureanu, P.K. Dutta, R. Partheniu, and E. Nastase. *Monitoring of radon and air ionization in a seismic area,* Rom. Rep. Phys. **69**, 709 (2017).
13. V.E. Toader, I.M. Popescu, I.A. Moldovan, and C. Ionescu. *Vrancea seismicity analysis based on cumulative seismic energy*, U.P.B. Sci Bull Ser A **77**, 297–308 (2015).
14. A. Gregorič, B. Zmazek, S. Džeroski, D. Torkar, and J. Vaupotič. *Radon as an Earthquake Precursor–Methods for Detecting Anomalies*, Earthquake Research and Analysis – Statistical Studies, Observations and Planning **01**, 179–196 (2012).